research papers

Crystal structure of CD59: implications for molecular recognition of the complement proteins C8 and C9 in the membrane-attack complex

Yuxiang Huang,[a] Alena Fedarovich,[b] Stephen Tomlinson[a]* and Christopher Davies[b]*

[a]Department of Microbiology and Immunology, Medical University of South Carolina, Charleston, SC 29425, USA, and [b]Department of Biochemistry and Molecular Biology, Medical University of South Carolina, Charleston, SC 29425, USA

Correspondence e-mail: tomlinss@musc.edu, davies@musc.edu

Human CD59 is a small membrane-bound glycoprotein that functions as an inhibitor of the membrane-attack complex (MAC) of the complement system by binding the complement proteins C8 and C9. The crystal structure of a soluble construct of CD59 has been determined to 2.1 Å resolution. When compared with previous models of CD59 determined using NMR, some interesting differences are noted, including the position of helix α1, which contributes to the binding surface for C8 and C9. Interestingly, the crystal structure superimposes more closely with an updated NMR model of CD59 that was produced using Monte Carlo minimization, including helix α1. Mapping of mutations associated with enhanced or lowered inhibitory function of CD59 show the binding region to be located in a crevice between α1 and a three-stranded β-sheet, as has been identified previously. Residues in the core of this region are well ordered in the electron density, in part owing to a network of stabilizing covalent and noncovalent interactions, and manifest an interesting 'striped' distribution of hydrophobic and basic residues. Docking of the same peptide that was modeled previously into the NMR structure shows that Arg55, which has been postulated to exist in 'open' and 'closed' positions, is intermediate in position between these two and is well placed to contact the peptide. Further clues regarding how CD59 interacts with small peptides arise from the crystal packing of this structure, which shows that a symmetry-related loop comprising residues 20–24 occupies a spatially similar position to the modeled peptide. This higher resolution structure of CD59 will facilitate a more precise dissection of its interactions with C8 and C9 and thus increase the likelihood of designing enhanced CD59-based therapeutics.

1. Introduction

Complement is an important effector mechanism of both innate and adaptive immunity and also plays an important role in enhancing the induction of humoral and cellular immune responses. The complement system is tightly controlled by various fluid-phase and membrane-bound complement-inhibitory proteins, most of which act at proximal activation steps in the complement cascade. The cytolytic membrane-attack complex (MAC) of complement is formed by the self-assembly of protein components C5b, C6, C7, C8 and multiple C9 molecules. CD59 is a membrane-bound glycoprotein that inhibits formation of the MAC by binding C8 and C9 in the nascent complex (reviewed in Morgan & Tomlinson, 2005).

Studies in rodent models implicate the MAC in many disease states and as an inhibitor of this complex CD59 appears to play an important protective role (Arumugam *et al.*, 2004; Morgan & Harris, 2003; Sahu & Lambris, 2000;

Quigg, 2002). Soluble forms of CD59 have shown therapeutic efficacy in rodent models of arthritis and renal injury (Fraser *et al.*, 2003; He *et al.*, 2005). In humans, deficiency of CD59 causes intravascular hemolysis that occurs in paroxysmal hemoglobinuria (PNH; Motoyama *et al.*, 1992; Yamashina *et al.*, 1990). CD59 is also overexpressed in many types of cancer and provides a mechanism for immune evasion by protecting tumor cells against antibody and complement attack (Fishelson *et al.*, 2003; Fonsatti *et al.*, 2000; Gelderman *et al.*, 2004; Caragine *et al.*, 2002).

More recently, several complement-independent roles for CD59 have been described. These roles include cell-signaling activities, LPS signaling, modulation of apoptosis and activities associated with the interaction of CD59 with CD2, calreticulin and the cytolysin of *Streptococcus intermedius* (reviewed in Kimberley *et al.*, 2007). Understanding the interactions between CD59 and its ligands is of considerable biological significance and will make the rational design of efficient CD59 inhibitors (*e.g.* for anti-cancer therapy) and improved CD59-based molecules (*e.g.* for anti-inflammatory therapy) more feasible.

Human CD59 comprises 77 amino acids and is linked to the plasma membrane *via* a glycophosphatidyl inositol (GPI) anchor. The mature protein contains a single N-linked glycosylation site at Asn18 and contains a limited degree of O-glycosylation (Rudd *et al.*, 1997). Glycosylation is not required for the complement-inhibitory activity of CD59 (Akami *et al.*, 1994; Yu *et al.*, 1997). NMR structures of the protein have been determined (Fletcher *et al.*, 1994; Kieffer *et al.*, 1994) and have confirmed that the fold of the protein is similar to that of the Ly6 superfamily of proteins (Williams, 1991). This fold comprises two antiparallel β-sheets, with a single α-helix packing against the larger three-stranded β-sheet. Mutational studies suggest that the binding interfaces for C8 and C9 overlap and lie within a surface depression of CD59 between the α-helix and the three-stranded β-sheet that is centered around Trp40 (Petranka *et al.*, 1996; Yu *et al.*, 1997; Bodian *et al.*, 1997; Hinchliffe & Morgan, 2000; Huang *et al.*, 2005, 2006). A short six-residue peptide corresponding to a CD59-binding region of C9 has been docked into this putative binding site (Huang *et al.*, 2006). Owing to the lack of a high-resolution structure of CD59, however, the details of the binding region and of the interactions with C8/C9 remain unclear. Here, we report the crystal structure of CD59 determined at 2.1 Å. This reveals the protein structure in considerable more detail than was possible previously and provides a better definition of the binding interface.

2. Experimental

2.1. Crystallization and X-ray data collection

Recombinant soluble CD59 was expressed in *Pichia pastoris* and purified by antibody-affinity and ion-exchange chromatography, as described previously (Huang *et al.*, 2006). This protein comprises residues 1–74 but also includes two non-native residues at the N-terminus that result from the

cloning. Compared with the sequence of the wild-type protein, it also contains an N18Q mutation at a site of glycosylation, which facilitates expression in *P. pastoris* but does not affect the activity of the protein (Yu *et al.*, 1997).

The protein was exchanged into PBS buffer and concentrated to 15 mg ml^{-1}. Crystallization trials were performed using the hanging-drop vapor-diffusion technique, in which 2 µl protein solution was mixed with 2 µl well solution. Preliminary crystals were obtained using PEG 6000 as a precipitant in the pH range 3.5–5.0. On the basis of improving the size and visible quality of the crystals, these conditions were optimized by altering the pH and the concentration of precipitant and by the inclusion of various additives. The best crystals were obtained in 10 µl drops over wells containing 0.1 *M* sodium citrate pH 3.5, 16% PEG 6000 and 5% 2-propanol incubated at 297 K. These grew as hexagonal rods with approximate dimensions of 0.1 × 0.1 × 1 mm. The crystals were cryoprotected by a quick passage through a solution containing 14% PEG 6K, 28% PEG 8K and 0.1 *M* sodium citrate pH 3.5. Preliminary diffraction analysis showed that the crystals belonged to point group *P*6, with unit-cell parameters *a* = *b* = 56.4, *c* = 39.4 Å. Examination of the systematic absences indicated the most likely space group to be *P*6$_3$. Calculation of the Matthews coefficient suggested there was one molecule of CD59 in the asymmetric unit (Matthews, 1968), corresponding to a solvent content of 49%.

Data were collected on a MAR225 CCD at the SER-CAT BM22 beamline at the Advanced Photon Source, Argonne National Laboratory, Chicago, IL, USA. The wavelength used was 1.75 Å in an attempt to phase the structure using the anomalous signal of the S atoms present in the molecule. Although this was unsuccessful (see below), these data were used to solve the structure and to refine the final model. In this experiment, the crystal-to-detector distance was 100 mm, the exposure time was 3.4 s per frame and 219° of data were collected in increments of 1.0°. The data were integrated and scaled with *HKL*-2000 (Otwinowski & Minor, 1997).

2.2. Structure determination and refinement

Initial attempts were made to solve the structure using the anomalous signal of sulfur. CD59 has a molecular weight of 8.9 kDa and contains ten S atoms present within cysteines, all of which form disulfide bridges. Attempts were made to phase the structure using *SnB* (Weeks & Miller, 1999) and *SOLVE* (Terwilliger & Berendzen, 1999). However, neither of these produced a satisfactory solution for the anomalous substructure and all attempts at phasing with *SOLVE* and *OASIS* (Hao, 2000) failed to produce an interpretable map. The possible reasons for this failure are described below.

The lack of success of SAD prompted an attempt to determine the structure by molecular replacement. NMR structures of CD59 are available (Kieffer *et al.*, 1994; Fletcher *et al.*, 1994) and the model 1cdq (Fletcher *et al.*, 1994) was used in molecular-replacement calculations using *Phaser* (McCoy *et al.*, 2005). Extensive calculations were performed at different resolutions, with various modifications of the search model

and testing all space groups of the $P6$ point group. The best solution was found in space group $P6_3$ at a resolution of 2.5 Å using a search model consisting of the first molecule in the NMR ensemble of 1cdq from which the C-terminal residues 76 and 77 had been omitted. The log-likelihood gain (LLG) of this solution was 19.9, with the next highest peak having a LLG of 13.9. Examination of the packing of this solution showed it to be free of any significant clashes.

The initial model was refined with *CNS* (Brünger *et al.*, 1998) and the resulting electron-density maps were used to adjust the model manually using *O* (Jones *et al.*, 1991). Thereafter, all refinements were performed with *REFMAC*5 (Murshudov *et al.*, 1997) interspersed with manual revision. In later rounds, water molecules were introduced using *ARP/wARP* (Lamzin *et al.*, 2001) and TLS refinement was also included in which one molecule of CD59 was defined as a rigid body. One of the non-native residues at the N-terminus was visible in the electron density and was added to the model as Phe0. In contrast, three (native) residues at the C-terminus were not visible and were excluded. Throughout the refinement, 5% of the data were set aside for calculation of the free *R* factor (Brünger, 1992). The final model was refined at a resolution of 2.12 Å resolution with an *R* factor of 18.0% (free

Table 1
Data-collection and refinement statistics.

Values in parentheses are for the last resolution shell of data.

Space group	$P6_3$
Unit-cell parameters (Å)	$a = b = 56.4$, $c = 39.4$
Resolution (Å)	28.2–2.1 (2.20–2.12)
No. of observations	50444
No. of unique observations	4118
Redundancy	12.2 (10.9)
Completeness (%)	99.3 (93.0)
$I/\sigma(I)$	52.9 (12.5)
R_{merge}† (%)	5.1 (14.1)
No. of protein atoms	608
No. of water molecules	96
R_{cryst} (%)	18.0
R_{free} (%)	25.4
R.m.s.d. bond length (Å)	0.010
R.m.s.d. bond angles (°)	1.44
Ramachandran statistics (%)	
Most favorable region	85.7
Additional allowed region	14.3
Generously allowed region	0.0
Disallowed region	0.0
Mean *B* factor, all atoms (Å^2)	22.7
R.m.s. deviation in *B* factors (Å^2)	
Main-chain atoms	0.38
Side-chain atoms	1.31

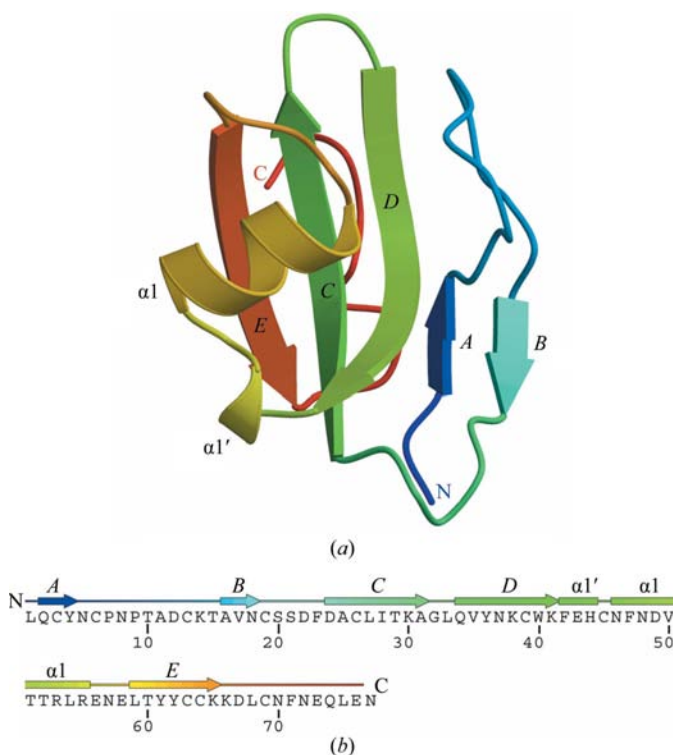† $R_{\mathrm{merge}} = \sum_{hkl} \sum_i |I_i(hkl) - \langle I(hkl) \rangle| / \sum_{hkl} \sum_i I_i(hkl)$.

R factor = 25.4%; Table 1). One possible reason for the relative gap between the *R* factor and the free *R* factor is the small size of the free *R* set. The total number of unique reflections in the data set was 4118 and 5% of these comprises only 189 reflections. In these circumstances, just a few poorly measured reflections can have a disproportionately large effect on the value of R_{free} and in hindsight a larger R_{free} set should have been used.

2.3. Attempt at sulfur phasing

The failure of the SAD approach to solve the structure using the sulfur signal was of interest because in theory, given the large number of sulfurs relatively to the molecular weight of the protein, CD59 ought to present an ideal case for this approach. Indeed, the estimated Bijvoet ratio at the wavelength used to collect the data is 1.2%, which is above the 0.6% threshold that is considered to be useful for phasing (Wang, 1985). In addition, the merging statistics of the data are very good (Table 1) and in the final refined model all the S atoms appeared to be fully occupied, arguing against oxidation of the sulfurs during the diffraction experiment being responsible.

Using the calculated phases derived from the final refined model, an anomalous difference Fourier electron-density map was calculated. This showed peaks of density near the disulfide bridges, confirming that a detectable anomalous signal was present in the data (not shown). In some cases, the two sulfurs of the disulfide were resolved into separate peaks, but for others the density was a single elongated peak that encompassed both sulfurs. The positions of the ten sulfurs in the refined model were then used in new phasing calculations using *SOLVE* or *OASIS*. Features of both of the resulting

(a)

N $\overset{A}{\longrightarrow}$ $\overset{B}{\longrightarrow}$ $\overset{C}{\longrightarrow}$ $\overset{D}{\longrightarrow}$ α1′   α1

LQCYNCPNPTADCKTAVNCSSDFDACLITKAGLQVYNKCWKFEHCNFNDV
         10   20   30   40   50

α1   E

TTRLRENELTYYCCKKDLCNFNEQLEN C
       60   70

(b)

Figure 1
The structure of human CD59. (*a*) The structure is displayed in ribbon format showing the secondary structure and is color-ramped from blue to red in the N-terminal to C-terminal direction. The elements of secondary structure are labeled according to previous NMR structures of CD59 (Fletcher *et al.*, 1994; Kieffer *et al.*, 1994). (*b*) The primary sequence of CD59 and the secondary-structure assignments derived from the crystal structure. Note that in the protein used in this study Asn18 was mutated to Gln to prevent glycosylation of the protein. This figure was produced with *MOLSCRIPT* (Kraulis, 1991), *RASTER3D* (Merritt & Murphy, 1994) and *SecSeq* (http://www.bioxray.dk/~deb/secseq/).

maps overlapped with the $2|F_o| - |F_c|$ map, suggesting that the solution was essentially correct, but neither map was of sufficient quality for model building. The same result was obtained when only the first 110° of data were used, arguing against radiation damage being the underlying problem. Recently, it has come to light that during the time when the data for this study were collected there was a problem with the BM22 monochromator that led to instability of the optics at lower energies. This may have caused a variation in the intensities that compromised the anomalous signal in the data. Using sulfur for SAD phasing is potentially a powerful technique, but because the signal is inherently low, its success relies on all parameters of the experiment being optimal and even

small errors will degrade the signal beyond utility. In our case, a small and previously undetected problem in the monochromator crystal was enough to reduce the signal and prevent successful phasing.

3. Results

3.1. Structure description

The crystal structure exhibits the same fold as previous structures of the same protein solved by NMR (Fletcher *et al.*, 1994; Kieffer *et al.*, 1994) and so will be described only briefly (Fig. 1). The protein is compact in shape and comprises three β-strands (C–E) arranged in a central sheet that is packed on one side by a helix ($\alpha1$) and on the other by the C-terminal and N-terminal regions. There is also a very small helix (termed $\alpha1'$) prior to $\alpha1$ that was not described in the original NMR structures. The N-terminal region is mostly irregular loop, but contains a small β-ribbon (strands A and B) that packs edge-on with the main β-sheet. The structure is stabilized by several disulfide bonds involving cysteines 3–26, 6–13, 19–39, 45–63 and 64–69, which were identified initially by biochemical studies (Sugita *et al.*, 1993) and subsequently observed in the NMR structures (Fletcher *et al.*, 1994; Kieffer *et al.*, 1994). These linkages all exhibit strong electron density, showing that they have formed correctly in the *P. pastoris* expression system.

The B factors of the structure are relatively low, indicating a well ordered molecule within the crystal. The highest B factors cluster at residues on the loop connecting strands C and D (residues 31–34). The higher resolution of the structure compared with previous NMR models reveals some of the interactions that contribute to the overall stability of the fold. For instance, the region around Trp40, a residue that is important for the function of CD59 (Bodian *et al.*, 1997; Yu *et al.*, 1997) and which is at the heart of the peptide-binding region (Huang *et al.*, 2005), is stabilized by a number of tertiary interactions (Fig. 2). Cys39, which is adjacent to Trp40, participates in a disulfide bridge with Cys19, thus connecting strand D to the AB hairpin. Similarly, the side chain of Lys38 hydrogen bonds to the carbonyls of Cys6 (which itself is linked by a disulfide bond to Cys13) and Pro7, which connects the middle of strand D to the carboxyl end of strand A. The side chain of Trp40 is positioned by hydrophobic
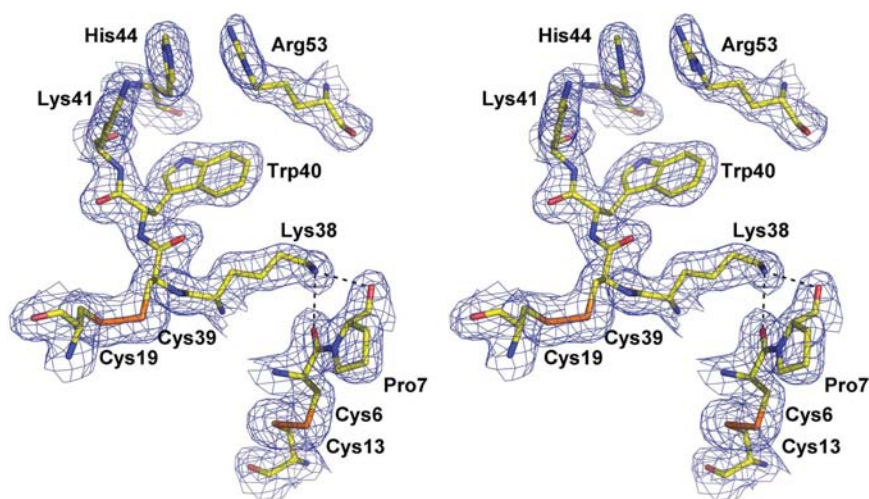
Figure 2
The electron-density map of CD59. In this stereoview, the $2|F_o| - |F_c|$ density is shown after the final crystallographic refinement, set against the refined model and contoured at 1σ. The region shown includes some of the residues that are important for the biological activity of CD59 (Trp40, His44 and Arg53), but also illustrates some of the disulfide bridges and hydrogen-bonding interactions that are likely to contribute to the stability of CD59.
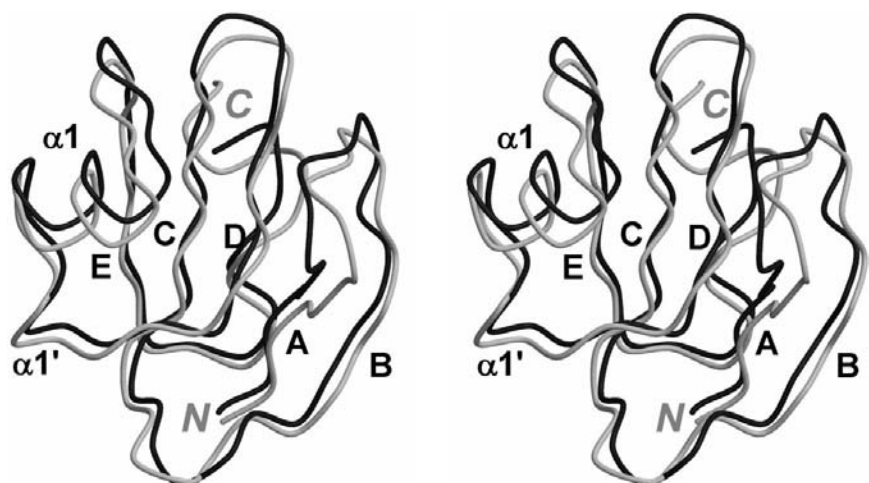
Figure 3
A comparison of CD59 with the same structure solved by NMR. The crystal structure of CD59 was superimposed with the first molecule of the ensemble comprising PDB entry 1cdq (Fletcher *et al.*, 1994) and each is shown in backbone form, with the crystal structure in black and the NMR model in gray. Secondary-structure elements are labeled in black and the termini are labeled in gray. This figure was produced with *MOLSCRIPT* (Kraulis, 1991) and *RASTER3D* (Merritt & Murphy, 1994).

packing against the aliphatic portions of the side chains of His44 and Arg53. Along with Lys41, these latter residues project prominently on the surface of CD59 and may be important for function.

3.2. Comparison with NMR-derived structures

The structure was compared with the first molecule of the NMR ensemble of CD59 (PDB code 1cdq; Fletcher *et al.*, 1994). The main-chain atoms of residues 1–74 could be superimposed with a root-mean-square (r.m.s.) deviation of 1.2 Å (Fig. 3). As expected, the closest overlap occurs in the β-sheet core of the protein. The most significant differences are in the relative positions of α1, the connecting loop between strands *A* and *B*, the crossover loop between *B* and *C*

and the C-terminal region. Most of these regions also show the highest structural differences within the NMR ensemble of 1cdq. The important exception to this, however, is helix α1 and its C-terminal connecting loop, which correspond very closely within the NMR ensemble, but are slightly shifted in the X-ray structure toward the main three-stranded β-sheet. The widest convergence occurs in residues 52–57 inclusive. This helix and connecting loop contribute several residues that are believed to be important for binding C8/C9 (see below).

Interestingly, the correspondence between structures is considerably higher when the crystal structure of CD59 is compared with that of an NMR model (PDB code 1cds) that was subject to a Biased Probability Monte Carlo minimization procedure (as implemented in *ICM*; Abagyan & Totrov, 1994; Huang *et al.*, 2005). In this case, the two structures superimpose with an r.m.s. deviation of 1.05 Å and, strikingly, α1 now overlaps more closely (not shown). Important residues such as Arg53, Asp22 and Trp40 also correspond more closely when comparing these two structures. Irrespective of which model most closely reflects the structure of CD59 in a physiological context, it is interesting to note how the modeling protocol shifted the NMR structure closer to that of the crystal structure.

3.3. C8/C9-binding site

Through a number of studies involving site-directed mutagenesis and loss-of-function assays, a putative binding site for C8 and C9 has been identified in CD59 (Bodian *et al.*, 1997; Yu *et al.*, 1997; Huang *et al.*, 2005). As noted previously, this is located in a crevice between helix α1 and strand *D* (Fig. 4). At the heart of this region is a hydrophobic 'stripe' comprising Leu54, Trp40 and Phe23 and bordered by the basic residues His44 and Arg53 (Fig. 4*b*). In the crystal structure, all of these residues exhibit strong electron density and low *B* factors, suggesting a rigid docking platform for C8 and C9. The stability of this region is probably enhanced by the disulfide bridge between Cys39 and Cys19 and the hydrogen bonds between the amino group of Lys38 and the main-chain carbonyls of Cys6 and Pro7 (see Fig. 2). Additional residues associated with loss of function of CD59 (Phe42 and Asp24) are located at the base of the molecule, as viewed in Fig. 4.

Some mutations (to alanine) enhance the inhibitory activity of CD59,
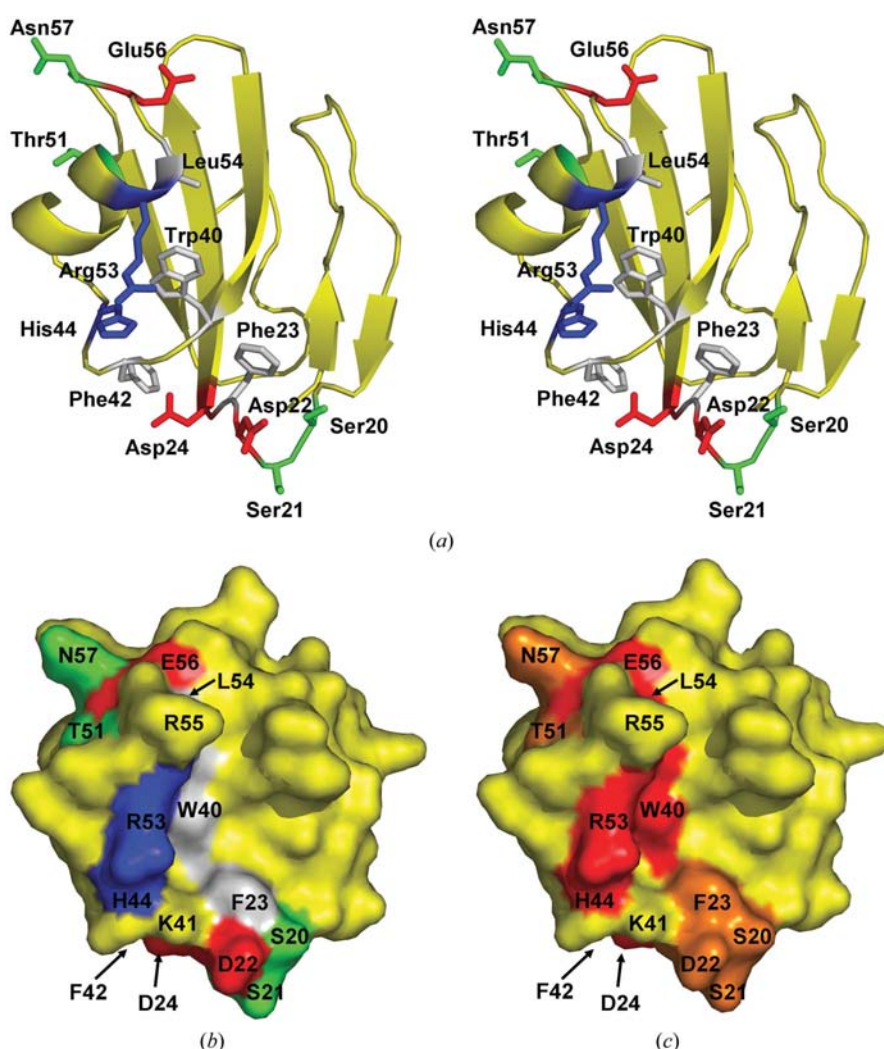
Figure 4
The putative C8- and C9-binding region of CD59. (*a*) In this stereoview, residues that have been shown to be important for the biological function of CD59 (see text for details) are shown in stick form set against a ribbon representation of the molecule in yellow. The residues are colored according to their respective physicochemical properties: hydrophobic residues are white, basic residues are blue, acidic residues are red and polar residues are green. (*b*) A surface representation of CD59 with the same view of the molecule as in (*a*) and with the same coloring scheme for important residues. (*c*) The same surface representation of CD59 as (*b*) but colored according to whether mutations lower (red) or enhance (orange) the inhibitory activity of CD59, as determined by Huang *et al.* (2005). This figure was produced with *PyMOL* (http://www.pymol.org).

including Asp22, Phe23, Thr29, Thr51 and Leu54 (Huang *et al.*, 2005). A second group of such mutants also show enhanced activity, albeit to a lesser extent, and include Ser20, Ser21, Leu27, Asn37, Arg53 and Asn57. Excluding those of residues that are buried within the hydrophobic core of the protein (Thr29, Leu27 and Asn37), these mutations extend the potential interaction surface of CD59 to encompass the loop between strands *B* and *C* at the base of the molecule and additional residues of helix α1 at the top left of the molecule (Fig. 4). Interestingly, the mutations map to two distinct patches (colored orange in Fig. 4c) that each border the central portion of the binding site (colored red) where mutations lower or abolish the inhibitory activity of CD59. Given its prominence at the heart of this binding region, it is surprising that mutation of Arg55 does not seem to affect the biological activity of CD59, at least in the context of its interaction with C8 and C9.

3.4. Docking of C9-derived peptide

Previously, a six-residue peptide (VSLAFS; numbered 2–7) was identified as the region of C9 that binds CD59 and was modeled into an NMR-derived model of CD59 (Huang *et al.*, 2006). To dock this peptide within the crystal structure of CD59, the peptide-bound model of CD59 was superimposed with the crystal structure (Fig. 5a). This shows that the crystal structure can accommodate the peptide without any significant alterations in its structure, including the side chain of Arg55, which had to be shifted when modeling the same peptide in the NMR-derived model of CD59 (Huang *et al.*, 2006). The only potential clash in the model is between Asn8 of CD59 and the side chain of Phe6 of the peptide, which is

caused by the different conformation of the connecting loop between strands *A* and *B* when comparing the crystal structure and the NMR-derived model of CD59.

Interestingly, examination of the crystal-packing interactions shows that the loop between strands *B* and *C* in a symmetry-related molecule of CD59 in the crystal lattice occupies a spatially similar region as the modeled peptide (Fig. 5b) and so could represent another model for how a peptide might bind to CD59. In support of this, some of the residues identified by site-directed mutagenesis as being important for the function of CD59 (Trp40, Arg53 and Leu54) are within contact distance of this loop. The closest contacts, however, involve the residues Lys38, Arg55 and Pro5. On the symmetry-related side, the residues that project into the crevice are Ser20, Ser21 and Asp22. Prominent amongst these is Ser21 and both its main-chain and side-chain atoms are within hydrogen-bonding distance of Lys38, Arg55 and Pro5.

4. Discussion

We have determined the structure of human CD59 using X-ray crystallography. As expected, this structure is broadly the same as previous NMR structures of the same protein (Fletcher *et al.*, 1994; Kieffer *et al.*, 1994). The main differences lie within those regions that vary within the NMR ensemble of models. The exceptions to this are helix α1 and its C-terminal loop, which overlap closely within the NMR ensemble but occupy shifted positions in the crystal structure. This is important because residues on this helix, such as Arg53 and Leu54, appear to play a major role in the binding of C8/C9 (Bodian *et al.*, 1997; Yu *et al.*, 1997). In the crystal structure, the C-terminal end of this helix is packed more closely into the

main body of the molecule compared with its position in the NMR structures. Thus, it is possible that such a helix exhibits some flexibility in solution and closes down upon binding of a protein partner such as C8 or C9. If so, then the 'closed' conformation of this helix may have been trapped in the crystal structure. Alternatively, the position of this helix in the crystal structure may simply be dictated by packing interactions in the crystal lattice. Indeed, examination of the packing shows this region to pack against strand *B* and the C-terminus of a symmetry-related molecule. Interestingly, a model that was generated from an NMR structure by Monte Carlo simulations (Huang *et al.*, 2005) converges more closely with the crystal structure than its progenitor model, including helix α1, even though this was produced in the absence of peptide.

The high degree of order in the crystal structure, as manifested by good electron density as well as low *B* factors,
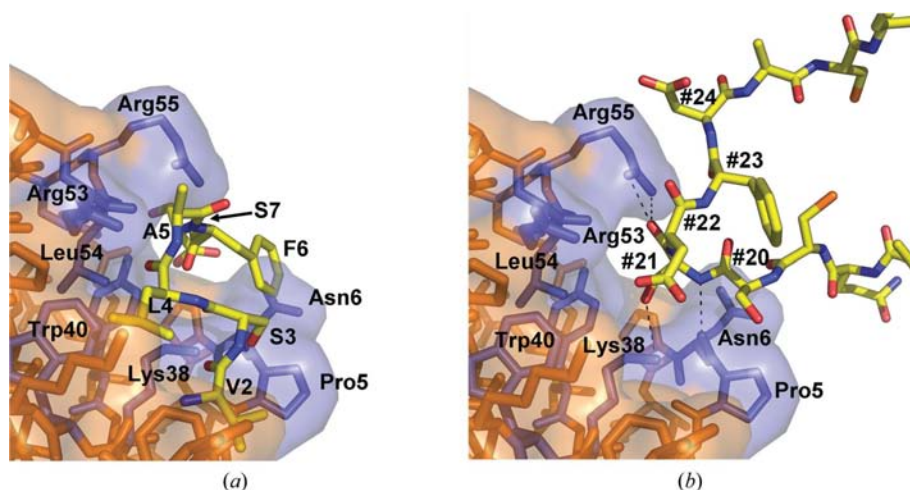
Figure 5
Two models for the binding of a peptide into the crystal structure of CD59. (a) Docking of the peptide comprising residues VSLAFS into the crystal structure by superimposition of the NMR-derived model of CD59 with the crystal structure. (b) The same view, but now showing how a loop from a symmetry-related molecule of CD59, comprising residues 20–24, binds into the same region of CD59. In both cases, CD59 is shown in stick form and is covered by a transparent surface. Residues and their respective surfaces that are within contact range of each peptide are colored blue. The remaining residues and surface of CD59 are both colored brown. Each 'peptide' is shown in stick form and is colored yellow. Residues involved in contacts are labeled using single-letter code for the peptide and residue number for the crystal-packing interaction (#, symmetry-related residue). This figure was produced with *PyMOL* (http://www.pymol.org).

has allowed a precise mapping of the binding surface of CD59. At the heart of this region are residues that were predicted from mutagenesis studies to be involved in binding C8 or C9, including Trp40 and Arg53. A very notable exception, however, is Arg55. This occupies a central location in the putative binding region and yet its mutation does not significantly affect the biological activity of CD59 (although in one study its mutation slightly enhanced the inhibitory activity of CD59; Huang *et al.*, 2005). This is all the more surprising because during a previous attempt to model a peptide (corresponding to C9) into CD59 the side chain of this residue had to be adjusted to avoid a steric clash (Huang *et al.*, 2006). Moreover, when docking the same peptide into the crystal structure, no adjustment to the side-chain Arg55 was required and this residue appears well placed to make hydrogen-bonding interactions with the peptide. The reason for this apparent discrepancy is not clear. One possibility is that Arg55 is important for binding other protein partners of CD59 such as the cytolysin intermedilysin, CD2 and calreticulin and plays a lesser role in the recognition of C8/C9. Another possibility is that the modeling of the peptide is only an approximation and lacks accuracy in the molecular details of how it might bind CD59. In fact, as our mapping shows and as was noticed previously (Huang *et al.*, 2006), the apparent epicenter of the binding surface of CD59 for C8/C9 is slightly below that of the modeled peptide (as viewed in Fig. 4).

Further clues as to how CD59 might recognize other proteins may be provided by the packing of molecules in the crystal lattice. Intriguingly, this shows that residues 20–22 of a neighbouring molecule project into the putative binding region of CD59 and may therefore mimic the binding of a peptide. In fact, some of the interactions, such as the potential hydrogen bonds between Ser21 (of the neighbouring molecule) and Lys38 and Pro5, appear to be very precise. Moreover, although the conformation of the peptide is different, the region of CD59 recognized *via* this symmetry-related interaction overlaps closely with that of the modeled peptide. Of course, the same criticisms of the modeled peptide then also apply to this model. Again, Arg55 appears to be an important residue in this mode of binding, which is contrary to the mutagenesis data, as is the key involvement of Lys38 and Pro7, which also have not emerged as important residues from scanning mutagenesis studies (Huang *et al.*, 2005). Another possibility, however, is that rather than representing how a C9-derived peptide binds CD59, this interaction may show how CD59 recognizes C8/C9, *i.e.* the involvement of residues 20–22 may mimic how that region of CD59 recognizes other proteins. As can be seen from Fig. 4, this region lies at the base of the molecule and is the site where mutations of Ser20 and Ser21 enhance the inhibitory activity of CD59. Such questions will be answered with the structure determination of complexes of CD59 with C8 or C9 or with peptides derived from those proteins.

References

Abagyan, R. & Totrov, M. (1994). *J. Mol. Biol.* **235**, 983–1002.

Akami, T., Arakawa, K., Okamoto, M., Akioka, K., Fujiwara, I., Nakai, I., Mitsuo, M., Sawada, R., Naruto, M. & Oka, T. (1994). *Transplant. Proc.* **26**, 1256–1258.

Arumugam, T. V., Shiels, I. A., Woodruff, T. M., Granger, D. N. & Taylor, S. M. (2004). *Shock*, **21**, 401–409.

Bodian, D. L., Davis, S. J., Morgan, B. P. & Rushmere, N. K. (1997). *J. Exp. Med.* **185**, 507–516.

Brünger, A. T. (1992). *Nature (London)*, **355**, 472–474.

Brünger, A. T., Adams, P. D., Clore, G. M., DeLano, W. L., Gros, P., Grosse-Kunstleve, R. W., Jiang, J.-S., Kuszewski, J., Nilges, M., Pannu, N. S., Read, R. J., Rice, L. M., Simonson, T. & Warren, G. L. (1998). *Acta Cryst.* D**54**, 905–921.

Caragine, T. A., Okada, N., Frey, A. B. & Tomlinson, S. (2002). *Cancer Res.* **62**, 1110–1115.

Fishelson, Z., Donin, N., Zell, S., Schultz, S. & Kirschfink, M. (2003). *Mol. Immunol.* **40**, 109–123.

Fletcher, C. M., Harrison, R. A., Lachmann, P. J. & Neuhaus, D. (1994). *Structure*, **2**, 185–199.

Fonsatti, E., Altomonte, M., Coral, S., De Nardo, C., Lamaj, E., Sigalotti, L., Natali, P. G. & Maio, M. (2000). *Clin. Ter.* **151**, 187–193.

Fraser, D. A., Harris, C. L., Williams, A. S., Mizuno, M., Gallagher, S., Smith, R. A. & Morgan, B. P. (2003). *J. Biol. Chem.* **278**, 48921–48927.

Gelderman, K. A., Tomlinson, S., Ross, G. D. & Gorter, A. (2004). *Trends Immunol.* **25**, 158–164.

Hao, Q., Gu, Y. X., Zheng, C. D. & Fan, H. F. (2000). *J. Appl. Cryst.* **33**, 980–981.

He, C., Imai, M., Song, H., Quigg, R. J. & Tomlinson, S. (2005). *J. Immunol.* **174**, 5750–5757.

Hinchliffe, S. J. & Morgan, B. P. (2000). *Biochemistry*, **39**, 5831–5837.

Huang, Y., Qiao, F., Abagyan, R., Hazard, S. & Tomlinson, S. (2006). *J. Biol. Chem.* **281**, 27398–27404.

Huang, Y., Smith, C. A., Song, H., Morgan, B. P., Abagyan, R. & Tomlinson, S. (2005). *J. Biol. Chem.* **280**, 34073–34079.

Jones, T. A., Zou, J.-Y., Cowan, S. W. & Kjeldgaard, M. (1991). *Acta Cryst.* A**47**, 110–119.

Kieffer, B., Driscoll, P. C., Campbell, I. D., Willis, A. C., van der Merwe, P. A. & Davis, S. J. (1994). *Biochemistry*, **33**, 4471–4482.

Kimberley, F. C., Sivasankar, B. & Morgan, B. P. (2007). *Mol. Immunol.* **44**, 73–81.

Kraulis, P. J. (1991). *J. Appl. Cryst.* **24**, 946–950.

Lamzin, V. S., Perrakis, A. & Wilson, K. S. (2001). *International Tables for Crystallography*, Vol. *F*, edited by M. G. Rossmann & E. Arnold, pp. 720–722. Dordrecht: Kluwer Academic Publishers.

McCoy, A. J., Grosse-Kunstleve, R. W., Storoni, L. C. & Read, R. J. (2005). *Acta Cryst.* D**61**, 458–464.

Matthews, B. W. (1968). *J. Mol. Biol.* **33**, 491–497.

Merritt, E. A. & Murphy, M. E. P. (1994). *Acta Cryst.* D**50**, 869–873.

Morgan, B. P. & Harris, C. L. (2003). *Mol. Immunol.* **40**, 159–170.

Morgan, B. P. & Tomlinson, S. (2005). *Structural Biology of the Complement System*, edited by D. Morikos & J. D. Lambris, pp. 251–264. Boca Raton: CRC Press.

Motoyama, N., Okada, N., Yamashina, M. & Okada, H. (1992). *Eur. J. Immunol.* **22**, 2669–2673.

Murshudov, G. N., Vagin, A. A. & Dodson, E. J. (1997). *Acta Cryst.* D**53**, 240–255.

Otwinowski, Z. & Minor, W. (1997). *Methods Enzymol.* **276**, 307–326.

Petranka, J., Zhao, J., Norris, J., Tweedy, N. B., Ware, R. E., Sims, P. J. & Rosse, W. F. (1996). *Blood Cells Mol. Dis.* **22**, 281–296.

Quigg, R. J. (2002). *Trends Mol. Med.* **8**, 430–436.

Rudd, P. M., Morgan, B. P., Wormald, M. R., Harvey, D. J., van den Berg, C. W., Davis, S. J., Ferguson, M. A. & Dwek, R. A. (1997). *J. Biol. Chem.* **272**, 7229–7244.

Sahu, A. & Lambris, J. D. (2000). *Immunopharmacology*, **49**, 133–148.

Sugita, Y., Nakano, Y., Oda, E., Noda, K., Tobe, T., Miura, N. H. & Tomita, M. (1993). *J. Biochem. (Tokyo)*, **114**, 473–477.

Terwilliger, T. C. & Berendzen, J. (1999). *Acta Cryst.* D**55**, 849–861.

Wang, B.-C. (1985). *Methods Enzymol.* **115**, 90–112.

Weeks, C. M. & Miller, R. (1999). *J. Appl. Cryst.* **32**, 120–124.

Williams, A. F. (1991). *Cell Biol. Int. Rep.* **15**, 769–777.

Yamashina, M., Ueda, E., Kinoshita, T., Takami, T., Ojima, A., Ono, H., Tanaka, H., Kondo, N., Orii, T., Okada, N., Inoue, K. & Kitani, T. (1990). *N. Engl. J. Med.* **323**, 1184–1189.

Yu, J., Abagyan, R., Dong, S., Gilbert, A., Nussenzweig, V. & Tomlinson, S. (1997). *J. Exp. Med.* **185**, 745–753.